

# Geophysical Research Letters®

## RESEARCH LETTER

10.1029/2025GL116116

### Key Points:

- We examine an anomalous zone of tectonic tremor offset 50–100 km west of the main tremor band at the southern edge of Cascadia
- We construct 27 stacked low-frequency earthquake (LFE) templates to facilitate detection and precise location of this activity
- LFEs form a northeast-dipping alignment at 22–29 km depth, plausibly indicating slip at the southern edge of subduction, ~15 km south of Gorda slab seismicity

### Supporting Information:

Supporting Information may be found in the online version of this article.

### Correspondence to:

D. R. Shelly,  
dshelly@usgs.gov

### Citation:

Shelly, D. R., Goldberg, D. E., Wech, A. G., & Thomas, A. M. (2025). A northeast-dipping zone of low-frequency earthquakes at the southern edge of Cascadia subduction. *Geophysical Research Letters*, 52, e2025GL116116. <https://doi.org/10.1029/2025GL116116>

Received 21 MAR 2025

Accepted 10 JUN 2025

Published 2025. This article is a U.S. Government work and is in the public domain in the USA. Geophysical Research Letters published by Wiley Periodicals LLC on behalf of American Geophysical Union.

This is an open access article under the terms of the Creative Commons Attribution-NonCommercial-NoDerivs License, which permits use and distribution in any medium, provided the original work is properly cited, the use is non-commercial and no modifications or adaptations are made.

## A Northeast-Dipping Zone of Low-Frequency Earthquakes at the Southern Edge of Cascadia Subduction

David R. Shelly<sup>1</sup> , Dara E. Goldberg<sup>1</sup> , Aaron G. Wech<sup>2</sup> , and Amanda M. Thomas<sup>3</sup>

<sup>1</sup>U.S. Geological Survey, Geologic Hazards Science Center, Golden, CO, USA, <sup>2</sup>U.S. Geological Survey, Volcano Science Center, Anchorage, AK, USA, <sup>3</sup>Department of Earth and Planetary Science, University of California, Davis, CA, USA

**Abstract** Tectonic tremor monitoring occasionally detects events in an anomalous zone in southern Cascadia, 50–100 km west of the main tremor band, near the expected southern edge of the subducting Gorda slab at the Mendocino triple junction. To investigate the geometry and temporal behavior of this tremor, we examine its constituent low-frequency earthquakes (LFEs) by developing 27 stacked LFE waveform templates that we use to detect events from 2018 to 2024. We then relocate LFE sources together with regional seismicity. We find that LFE hypocenters form a northeast-dipping alignment at 22–29 km depth, extending eastward from a zone of micro-earthquakes, ~15 km south of the southern edge of Gorda slab seismicity. These LFE families exhibit small bursts of activity every few days. Considering the strong world-wide association of tremor and LFEs with high slip-rate, plate-bounding faults, we hypothesize these LFEs may mark the southern edge of Cascadia subduction.

**Plain Language Summary** Tectonic tremor is a long-duration, low-amplitude ground vibration produced by slow slip on faults. In the Cascadia subduction zone, tremor mainly occurs in a long band stretching from north to south, but occasionally minor activity is detected in an anomalous zone in northern California at the southern end of Cascadia offset 50–100 km westward of the main band. To investigate the significance of this zone, we isolate 27 sources of low-frequency earthquakes (LFEs) within the tremor. Based on the waveforms of these events, we precisely locate these LFE sources and analyze their occurrence patterns from 2018 to 2024. Our results show that these events occur at depths of 22–29 km, forming a northeast-dipping alignment that extends eastward from a cluster of small earthquakes. Unlike the larger, periodic tremor bursts observed elsewhere in Cascadia, these LFEs occur in small, frequent bursts every few days. Given that LFEs and tremor are typically linked to slow slip, we propose that these events may mark the southernmost extent of Cascadia subduction.

## 1. Introduction

The Cascadia subduction zone along the Pacific coast of North America hosts a broad zone of tremor (Rogers & Dragert, 2003; Wech & Creager, 2008), associated low-frequency earthquakes (LFEs) (Bostock et al., 2012; Plourde et al., 2015; Royer & Bostock, 2014; Sweet et al., 2014; Thomas & Bostock, 2015), and episodic slow slip (Dragert et al., 2001; Miller et al., 2002) downdip from the highly coupled megathrust zone. Tremor and LFEs are thought to be generated by thrust-type slip on the subduction interface (Ide et al., 2007; Shelly et al., 2006; Wech & Creager, 2007). LFEs are so-named because they are generally depleted in high frequency energy compared to typical earthquakes of similar magnitude, but their identification usually relies on their repeated bursts of activity, often coinciding with time periods of identified longer-duration tremor signals (Shelly et al., 2007). LFE occurrence has also been shown to be synced with the timing of slow slip (Frank, 2016).

At Cascadia's southern end lies the Mendocino triple junction, where the Pacific, North American, and Gorda plates meet. This marks the transition from subduction to the north to San Andreas system transform motion to the south (Figure 1). Accordingly, the Mendocino triple junction hosts high rates of seismicity (Smith et al., 1993). Much of this seismicity is concentrated within the Gorda plate itself, sometimes referred to as the Gorda deformation zone (Wilson, 1989), as a result of north-south compression west of the triple junction, imparted by the northward-migrating Pacific plate. Despite substantial advances in our understanding of this complex tectonic region over past decades, fundamental features remain poorly constrained. Notably, debate continues regarding the location of the southern edge of Gorda subduction, the existence of a possible slabless window or a partially subducted fragment of oceanic crust southeast of the triple junction (e.g., Bohannon & Parsons, 1995; Furlong

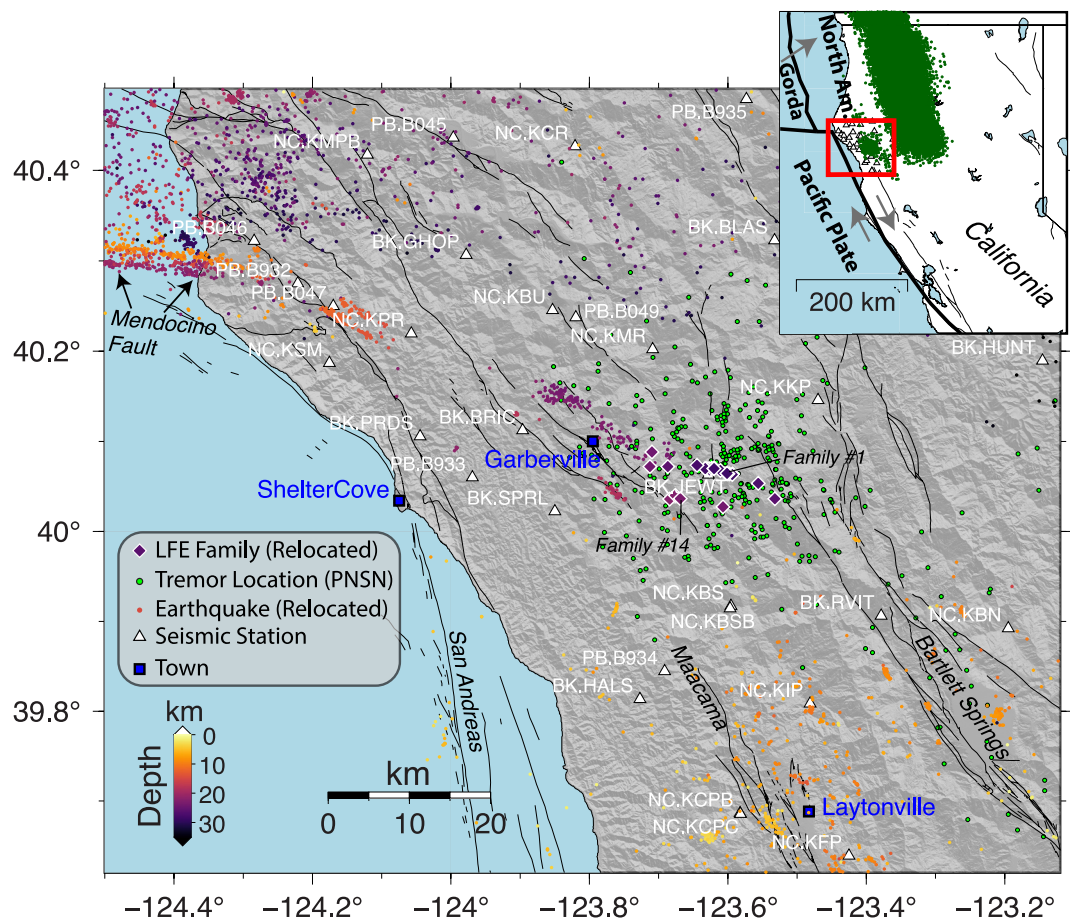


**Figure 1.** Map of relocated low-frequency earthquakes sources (white-outlined diamonds) and relocated earthquakes (01 January 2015–11 October 2024, dots), color-coded by depth. Green circles show Pacific Northwest Seismic Network (PNSN) tremor locations for 01 January 2020–31 July 2024. Black lines show faults from the Quaternary Fault and Fold Database (Data and Resources), with major fault zones labeled. Seismic stations shown as triangles. Inset shows location of map view (red box) along the broader distribution of PNSN tremor locations (dark green dots) in northern California. Bold black lines indicate plate boundaries and gray arrows indicate approximate relative plate motions.

et al., 2024; Hole et al., 1998; Verdonck & Zandt, 1994), and the way in which the San Andreas system (including San Andreas, Maacama, and Bartlett Springs faults) transitions at its northern end (e.g., Castillo & Ellsworth, 1993; Hole et al., 1998).

The main band of Cascadia tremor extends along most of the margin, with large episodes recurring every ~10–20 months depending on location (Brudzinski & Allen, 2007; Szeliga et al., 2004). Wech (2021) identified an anomalous zone of activity at the southern end of Cascadia near the Mendocino triple junction, offset 50–100 km west of the main tremor zone (Figure 1). Wech (2021) suggested that this tremor might relate to transform slip on the southern edge of the Gorda plate, but tremor locations were too uncertain to resolve the geometry of the host fault. As noted by Wech (2021), this zone is distinct from zones with LFE activity farther south reported by Plourde et al. (2015) associated with crustal strike-slip faults in the San Andreas fault system.

In this study, we investigate the anomalous Mendocino tremor zone in greater detail by developing 27 stacked LFE waveform templates, precisely locating each source to determine the underlying geometry, and applying template matching with continuous seismic data to analyze temporal behavior. Unlike traditional tremor location, which relies on the timing of amplitude variations in long-duration waveform envelopes (Wech & Creager, 2008), LFE analysis provides much higher precision in source location by utilizing both *P*- and *S*-phase arrival times. This approach also enables the detection of many more events through matched filter techniques (Gibbons & Ringdal, 2006), providing for a more comprehensive assessment of seismic activity in this region. By analyzing

continuous seismic data from 2018 to 2024, we identify patterns of LFE occurrence, shedding light on the spatial structure and temporal characteristics of tremor in this anomalous zone.

## 2. Methods

We developed LFE templates using a multi-step, iterative procedure of cross-correlation of candidate templates, stacking the detections with the highest correlation sum across the network, and picking phase arrivals (*P* and *S*) on the stacked waveforms. The stacked waveforms are then used to construct new templates with higher signal-to-noise ratios, with the process repeating. Our approach here was based on the approach developed by Shelly and Hardebeck (2010) for analysis of San Andreas Fault LFEs. The methods are briefly summarized here; full methods are available in Supporting Information S1.

In the present study, we developed 27 separate waveform templates (families). Although largely arbitrary, this number was chosen as sufficient to collectively detect activity during the 2018–2024 episodes of tremor identified in this area by Pacific Northwest Seismic Network (PNSN) monitoring in this area (PNSN.org/tremor). We formed initial waveform templates by manual selection of waveforms during times of PNSN-detected tremor in this area. In many cases, including the example shown in Figure 2, multiple nearby time windows were tried as templates; we retained the one that produced the strongest detections at other times.

Iterative detection and stacking (2–3 iterations) greatly improved the signal-to-noise ratio of the waveform templates (Figure 2). The higher signal-to-noise permitted identification of *P* and *S* phase arrival times, as well as improved detection of events.

After picking, we determined initial locations for each family using a grid search for minimum mean residual using the layered *P*-wave velocity model from Yoon and Shelly (2024), following the approach of Shelly and Hardebeck (2010). We refined these locations with *hypoDD* (Waldhauser & Ellsworth, 2000), using differential times derived both from phase pick times and from waveform cross-correlation. We relocated the LFE families together with nearby seismicity from 01 January 2015 to 11 October 2024, using phase pick times obtained from the Northern California Earthquake Data Center (NCEDC).

We also performed an initial exploration of geodetic data related to LFE activity (Supporting Information S1), inspired by successful efforts elsewhere to stack geodetic signals related to tremor and LFE activity (e.g., Frank, 2016; Rousset et al., 2019). Although this initial attempt was unsuccessful in resolving any deformation related to the LFE activity, future efforts could be important for constraining the associated slip magnitude and orientation. However, the geodetic moment associated with LFEs in this area may be small compared to subduction zone interfaces, where tremor and LFEs have been observed to be concurrently active over a much larger area.

## 3. Results and Discussion

Double-difference-relocated hypocenters reveal that the 27 LFE family hypocenters form an arcuate alignment at 22–29 km depth, extending nearly 20 km along a strike of ~290° and dipping toward the north-northeast at approximately 45° (Figure 3). Within this zone, the majority of the identified LFE families locate near the downdip edge and in the middle along strike, with more distributed sources on the updip, western, and eastern edges. Due to their close locations, the densely distributed families often contain overlapping detections, where multiple waveform templates detect the same event in the data. In this case, when an overall catalog is compiled, we retain only the detection with highest correlation sum within each 4 s window.

The zone of LFEs is also nearly aligned with a zone of mid-crustal seismicity that has been persistently active over time (Castillo & Ellsworth, 1993; Verdonck & Zandt, 1994). This zone of seismicity extends another ~15 km toward the west at slightly shallower depths, beneath the town of Garberville (Figure 1) and forms an apparent shallow-moderate dip to the northeast (Figure 3).

LFE source locations could benefit from use of a three-dimensional (3D) velocity model; however, based on experience elsewhere, the differences in locations would likely be minor, particularly for relative locations. For example, even in the Parkfield, California region, with a strong velocity contrast across the fault, locating with a 3D velocity model produces only minor differences in the patterns of earthquake hypocenters compared those produced with a one-dimensional (1D) velocity model (Thurber et al., 2006). For the 2022 magnitude (M) 6.4

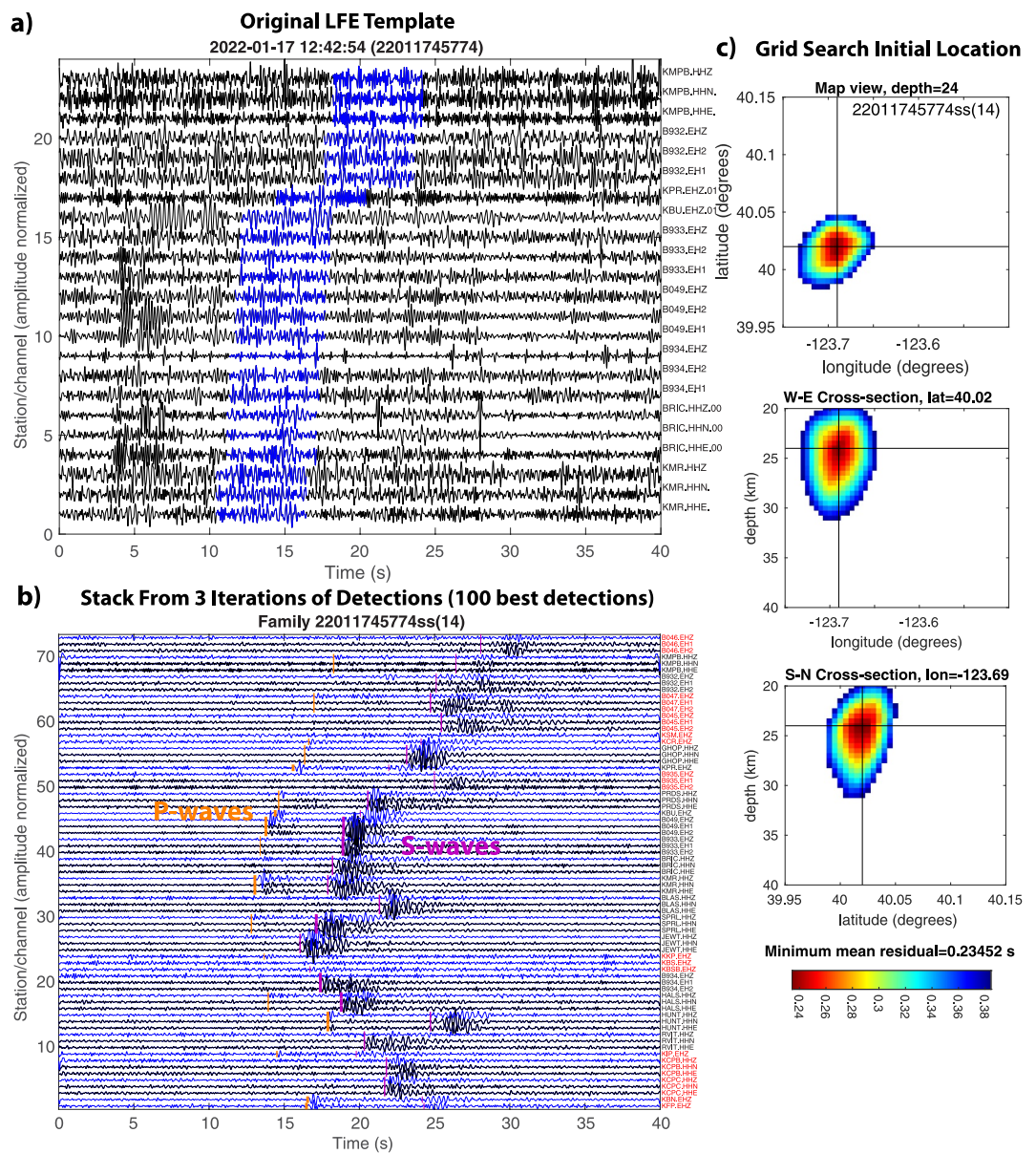


**Figure 2.** Example low-frequency earthquake (LFE) template development and initial location, shown for family #14. (a) Original candidate LFE waveform (6 s) is highlighted in blue (note that no LFE is visually apparent on most channels). Station and channel codes are indicated at right. Waveforms are filtered 2–9 Hz. (b) Waveforms obtained from three iterations of detections and stacking. Note the inclusion of many additional channels of data that were unavailable for original template but available for other similar events. Channels added in the final stacking (only used in stacking and not for event detection) are labeled at right in red. Manual phase picks are indicated for P (orange) and S (purple) arrivals. (c) Initial hypocenter location obtained using grid search with the phase picks shown in panel (b), with map view (top), west-east cross-section (middle), and south-north cross-section (bottom).

Ferndale earthquake in the Mendocino region, relocation using a 3D velocity model resulted in slightly shallower hypocenter estimates but very similar patterns of relative locations compared to those performed using a 1D model (Guo et al., 2024).

The temporal occurrence patterns show small bursts of activity every few days in each family, with a typical recurrence time of only about 2 days (Figure 4). Only minor variation is observed among families, with some families having slightly longer recurrence times. This behavior and recurrence time is similar to that observed for the least episodic families along the San Andreas Fault (Shelly & Johnson, 2011), consistent with the LFE sources

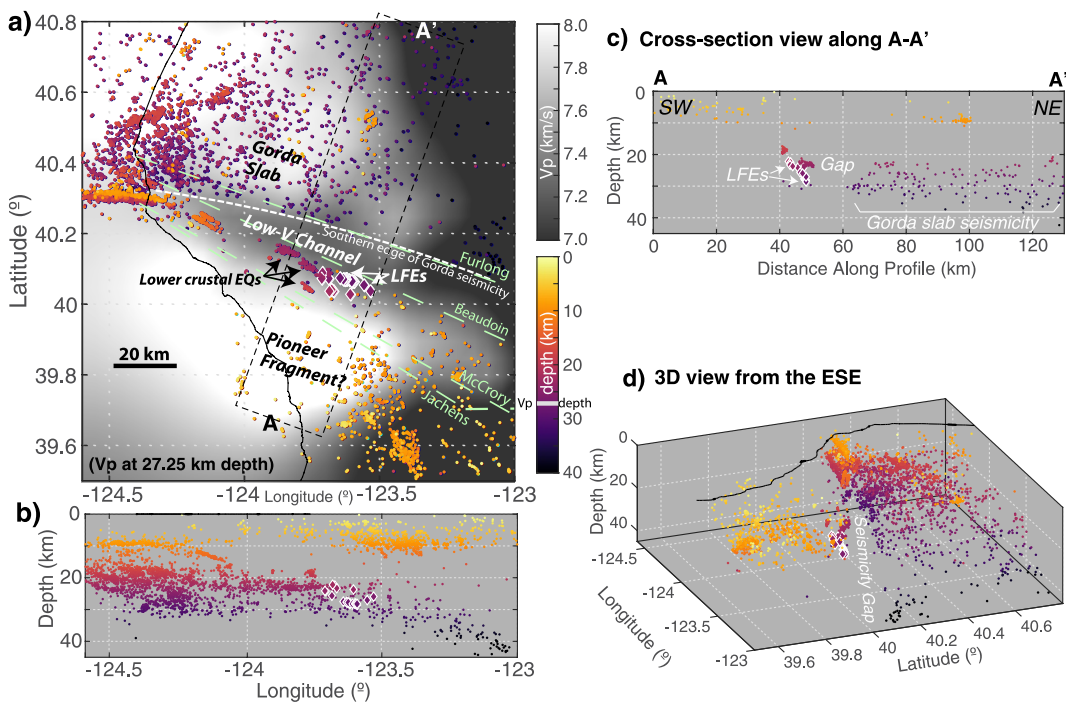


**Figure 3.** Relocated low-frequency earthquake (LFE) families and microseismicity. Microseismicity is from 01 January 2015 to 11 October 2024 (see Methods). LFEs are shown by white-outlined diamonds. Other seismicity shown by dots, color-coded by depth. Bold black line indicates the coastline. (a) Map view. Dashed box A-A' indicates the area of the cross section plotted in part (c).  $P$ -wave velocity ( $V_p$ ) depth slice at 27.25 km depth (near the mean LFE depth) from Furlong et al. (2024). Note that LFEs and microseismicity occur along a pronounced velocity contrast, tracking the southern boundary of the low-velocity (low-V) channel. Previously proposed edges of the Gorda slab are shown by light green dashed lines, labeled (from north to south) as Furlong (Furlong et al., 2024), Beaudoin (Beaudoin et al., 1998), McCrory (McCrory et al., 2006), and Jachens (Jachens & Griscom, 1983). The interpreted southern edge of Gorda slab seismicity is indicated by the slightly curved white dotted line. Velocity scale is truncated to emphasize relevant features. (b) West-east cross section, showing all events. (c) Cross section view along the line A-A' (oriented along an azimuth of 20°), showing the dipping alignment of LFEs on the eastern edge of a zone of microseismicity. Seismicity is plotted from within the 30-km-wide dashed box in panel (a). (d) Three-dimensional view from the east-southeast (from azimuth 112° and elevation 22°), showing the gap in seismicity between LFEs and Gorda slab seismicity to the north.

being surrounded by nearly steady, ongoing fault creep. Notably absent from our data set are any families that exhibit large, infrequent bursts of activity associated with episodic slow slip events, as observed for much of the main Cascadia zone (Wech & Creager, 2011) and for a subset of San Andreas LFE families.

We also observe frequent episodes of migration among LFE sources. Figure 4d shows one prominent example with migration velocities of ~40–80 km/hr, similar to velocities observed for tremor and LFEs in Cascadia (Ghosh et al., 2010), the Nankai subduction zone (Shelly et al., 2007), and the San Andreas Fault (Shelly, 2010). Most of the bursts (Figure 4c) exhibit some degree of migration among different sources, although the migration coherence and propagation distance varies.

The LFE activity may help illuminate the complex tectonics at the Mendocino triple junction. Worldwide, observations of tremor and LFEs have a strong association with major plate-bounding faults. In addition to numerous observations on the downdip portion of subduction megathrust faults (Beroza & Ide, 2011), LFEs are also generated by strike-slip motion along downdip extension of the San Andreas Fault in California (Shelly & Hardebeck, 2010) and the Alpine fault in New Zealand (Chamberlain et al., 2014; Wech et al., 2012), as well as by thrust motion in the Taiwan Central Range, possibly reflecting subduction of the Eurasian Plate (Ide et al., 2015). Thus, combined with their rapid recurrence, it is likely that the Mendocino LFEs are also associated with plate boundary motion. However, the northeast-dipping geometry of the Mendocino LFE sources (Figure 3c) is inconsistent with occurrence on the subduction megathrust. What then is their tectonic significance?

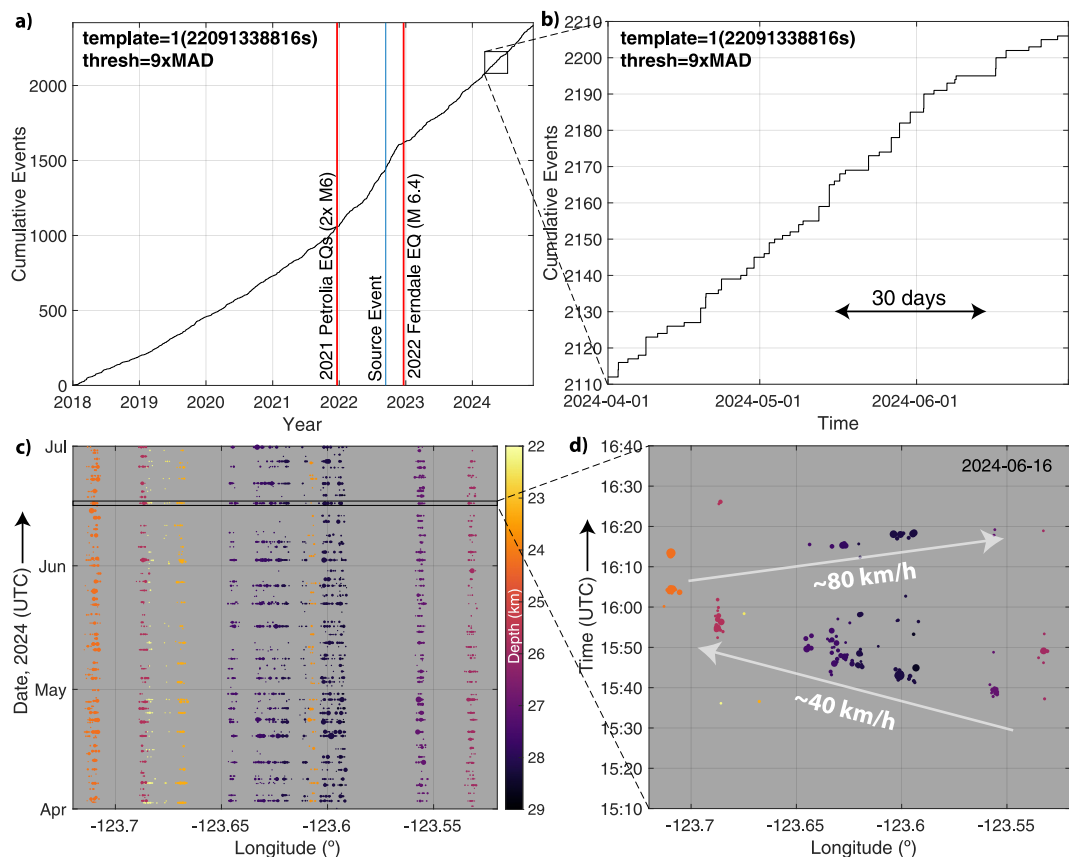


**Figure 4.** Temporal patterns of low-frequency earthquake (LFE) activity. (a) Example of cumulative events detection timeseries for LFE family #1 (Figure 1) using a correlation sum detection threshold of 9 times daily median absolute deviation, 01 January 2018–30 November 2024. Minor variations in detection rate over time may relate to network performance (Figure S1 in Supporting Information S1), with no obvious response to the marked nearby earthquakes (red lines). (b) Zoomed view of 3 months of cumulative events from panel (a) showing small bursts of events separated by a few days. (c) LFE occurrence time versus longitude for a 3-month period in 2024, showing activity in all 27 families. Marker size scales with detection strength (correlation sum) and is colored by family depth. A small random dither is applied to the family longitude value for improved visualization. Black dashed lines indicate the time shown in panel (d). (d) Zoomed view of (c) showing 1.5 hr on 16 June 2024, with an example of LFE migration along strike. Reference velocities of 40 and 80 km/hr are shown.

The location of the southern edge of the Gorda slab has been debated for decades (Figure 3a). Jachens and Griscom (1983) modeled gravity data to infer a relatively southern extent of the slab, extending from the triple junction with a strike of  $\sim 120^\circ$ . However, this southern extent has been refuted, with Furlong and Govers (1999) arguing that the associated gravity anomaly might instead be derived from a flexural downwarp in the crust. Meanwhile, McCrory et al. (2006) estimated the southern edge of the slab as directly below the boundary between compressional and dilatational  $P$ -wave first motions from an offshore earthquake on the Mendocino transform fault. This estimate was similar to the southern extent estimated by Jachens and Griscom (1983), but it did not account for possible lateral refraction of seismic waves along the slab edge. A more northerly estimate for the southern edge of the Gorda slab was inferred based on the southern edge of intraslab seismicity (Smith et al., 1993) and seismic velocity structure from earthquake tomography (Furlong et al., 2024; Verdonck & Zandt, 1994), with a proposed strike of  $\sim 105^\circ$  from the triple junction. Beaudoin et al. (1998) used active source seismic imaging and gravity modeling, estimating an intermediate location for the southern edge of the slab, striking at  $\sim 115^\circ$ . Currently available slab models (Hayes et al., 2018; McCrory et al., 2012) have adopted the relatively southerly estimate from McCrory et al. (2006). Of course, these varied estimates may map different properties (including density, seismic velocity, seismic reflectivity, or seismic activity) (Nuyen & Schmidt, 2024) or be sensitive to different depths, which could lead to a different map-view boundary, given the potential for a non-vertical slab edge.

The Mendocino LFEs lie within this broad range of slab edge estimates, lending plausibility to the hypothesis that they might be generated by slip on the slab edge (Wech, 2021). In particular, the LFE sources lie very close to the slab edge proposed by Beaudoin et al. (1996, 1998) based on active-source seismic data and gravity modeling (Figure 3a). Beaudoin et al. (1996) observed that seismicity terminated north of their proposed slab edge, which, along with changes in seismic reflectivity, they attributed to changes in either lithology or slab continuity. Seismic velocity models show a ~15 km-wide aseismic zone of pronounced low-*P*-velocity separating the LFEs and slab seismicity at depths between 20 and 30 km (Furlong et al., 2024; Verdonck & Zandt, 1994). Figure 3a shows the relationship between relocated seismicity and a slice of the Furlong et al. (2024) *P*-wave velocity model at 27.25 km depth, near the predominant depth of LFE sources. This low-velocity zone has been suggested to represent tectonically thickened crust, likely subduction complex material (Verdonck & Zandt, 1994) or perhaps crustal thickening related to the northward migration of the triple junction (Furlong & Govers, 1999).

The ongoing northward migration of the Mendocino triple junction and Gorda slab could create a slabless window (Beaudoin et al., 1996, 1998; Dickinson & Snyder, 1979; McCrory et al., 2009) where upwelling aesthenospheric mantle might fill the void at the southern edge of the northward-migrating Gorda slab. However, based on tectonic reconstructions and a high *P*-wave velocity zone observed in tomographic studies southeast of the triple junction, it has also been proposed that a portion of the Pacific plate may be underthrust beneath westernmost North America (Verdonck & Zandt, 1994) or that a fragment of the subducted Farallon plate may have become captured by the Pacific plate and be translating northward with the Pacific plate (Bohannon & Parsons, 1995). The fragment that is hypothesized to lie south of the subducted Gorda slab has been termed the “Pioneer fragment” (Furlong et al., 2003, 2024; McKenzie et al., 2022). Notably, the LFEs align along the northern edge of the high-velocity zone of the hypothesized Pioneer (Figure 3a). However, the nature of this zone and its present tectonics remain highly uncertain.

The LFE alignment (strike ~290) is distinct from the much more northerly strike of faults in the San Andreas system (Figure 1), making it unlikely that the LFEs are directly associated with San Andreas system transform motion. In fact, relative motion between the Pacific and North American plates would imply oblique reverse and right lateral strike-slip motion on a fault adopting the LFE alignment. This also seems unlikely, as this would imply northwestward subduction of the Pioneer fragment beneath the North American plate, and no evidence of such behavior has been reported from tomographic (or other) studies (e.g., Furlong et al., 2024; Verdonck & Zandt, 1994).

In our interpretation, the most likely scenarios would imply a direct relation between LFE activity and Cascadia subduction, accommodating relative motion between the Gorda plate and either North-American-like or Pacific-like motions. If the Pioneer fragment is simply accreted to the North American plate, then we might observe normal faulting on the LFE alignment, as the Gorda plate diverges to the northeast. Although this hypothesis seems plausible, it is difficult to understand as a stable, long-term configuration, given that it would imply continued downdropping of the southern Gorda slab. However, if the Pioneer is indeed captured by the Pacific as has been proposed (Bohannon & Parsons, 1995; Furlong et al., 2024), the LFEs might reflect relative Gorda-Pacific motion, accommodated by dipping right-lateral strike slip motion following the LFE alignment of ~290°. Either Gorda-related scenario would imply that the LFEs occur along the southern edge of subduction and that the low-velocity zone is accreted to the upper southern edge of the Gorda plate. This low-velocity zone might reflect subducted material accumulated above the south-dipping trailing edge of the northward migrating Gorda slab (Figure 3).

#### 4. Conclusions

We developed and located a set of 27 LFE families near the Mendocino triple junction, distinct from the main band of Cascadia tremor. Dipping to the northeast at 22–29 km depth, their tectonic role is currently uncertain, but they may demarcate the southern limit of subduction. Their activity could eventually help to untangle the extremely complex tectonics of this region, including the nature of the high velocity zone southeast of the triple junction corresponding to the proposed Pioneer fragment.

Further insight into this geometry could be provided by constraints on the LFE slip orientation, as initial attempts have thus far proven unsuccessful. Multiple avenues exist for future exploration of the slip associated with these LFEs, including analysis of *P*-wave first motion polarities, further attempts to stack geodetic observations (Frank, 2016), stacking of long-period energy associated with tremor bursts to compute moment tensors

(Ide, 2016; Ide & Yabe, 2014), and modeling of LFE tidal modulation (Thomas et al., 2012). Each has distinct challenges, generally contending with very low signal-to-noise and the possibility that their slip may be accompanied, influenced, or even controlled by slip on the nearby subduction thrust.

In addition to illuminating complex tectonics, LFE families could also provide a new metric of ongoing fault slip at depth at the southern edge of Cascadia. Given their frequent recurrence, typically every 2–3 days in each family, they present a tantalizing means for monitoring ongoing slip in region, which is not resolvable by other means. The analysis presented here goes back to 2018, due to station availability, but the stacked waveforms with the expanded station set used in this study for hypocentral locations might facilitate monitoring back to at least 2009, when most of the PB network borehole seismometers (<https://www.fdsn.org/networks/detail/PB/>) became operational (Figure 1). The current seismic network is well suited to continued monitoring of these LFE sources into the future.

Notably, because this LFE activity occurs westward of the main Cascadia tremor zone, it is directly adjacent to the expected seismogenic zone, which is capable of generating magnitude-9-class earthquakes. Ongoing LFE monitoring could reveal any future periods of accelerated activity in this area, potentially contributing to time-dependent assessments of earthquake hazard in Cascadia.

## Data Availability Statement

The full catalog of LFE detections is available in Shelly (2025). Waveform, phase, and event catalog data were obtained from the Northern California Earthquake Data Center (NCEDC), [needc.org](http://needc.org), doi: [10.7932/NCEDC](https://doi.org/10.7932/NCEDC) and the EarthScope Seismological Facility for the Advancement of Geoscience (SAGE) Data Management Center (<https://ds.iris.edu/ds/nodes/dmc/>, last accessed 28 February 2025). Global Navigation Satellite System (GNSS) data were acquired from the EarthScope Geodetic Facility for the Advancement of Geoscience (GAGE) facility (<https://www.unavco.org/data/gps-gnss/gps-gnss.html>, last accessed 28 February 2025). Figure 1 was created using Generic Mapping Tools version 6 (Wessel et al., 2019), with fault information from the U.S. Geological Survey and California Geological Survey, Quaternary fault and fold database for the United States, accessed 01 December 2021, at: <https://www.usgs.gov/natural-hazards/earthquake-hazards/faults>. The *P*-wave velocity model was obtained from Benz (2024).

## Acknowledgments

Stations used in this study are operated by the U.S. Geological Survey (NC network, doi: [10.7914/SN/NC](https://doi.org/10.7914/SN/NC)), UC Berkeley (BK network, doi: [10.7932/BDSN](https://doi.org/10.7932/BDSN)), and the Earthscope Consortium (PB network, <https://www.fdsn.org/networks/detail/PB/>, last accessed 12 May 2025). We thank William Frank, Jeanne Hardebeck, and Nathaniel Miller for very helpful reviews, as well as Kathryn Materna, Bob McPherson, and Jay Patton for enlightening discussion and comments. Any use of trade, firm, or product names is for descriptive purposes only and does not imply endorsement by the U.S. Government.

## References

- Beaudoin, B. C., Godfrey, N. J., Klemperer, S. L., Lendl, C., Trehu, A. M., Henstock, T. J., et al. (1996). Transition from slab to slabless: Results from the 1993 Mendocino triple junction seismic experiment. *Geology*, 24(3), 195–199. [https://doi.org/10.1130/0091-7613\(1996\)024<195:TFSTSR>2.3.CO;2](https://doi.org/10.1130/0091-7613(1996)024<195:TFSTSR>2.3.CO;2)
- Beaudoin, B. C., Hole, J. A., Klemperer, S. L., & Tréhu, A. M. (1998). Location of the southern edge of the Gorda slab and evidence for an adjacent asthenospheric window: Results from seismic profiling and gravity. *Journal of Geophysical Research*, 103(B12), 30101–30115. <https://doi.org/10.1029/98JB02231>
- Benz, H. M. (2024). Formation and Evolution of the Pacific–North American (San Andreas) Plate Boundary: Constraints from the Crustal Architecture of Northern California [Dataset]. *U.S. Geological Survey data release*. <https://doi.org/10.5066/P14QGYIY>
- Beroza, G. C., & Ide, S. (2011). Slow earthquakes and nonvolcanic tremor. *Annual Review of Earth and Planetary Sciences*, 39(39), 271–296. <https://doi.org/10.1146/annurev-earth-040809-152531>
- Bohannon, R. G., & Parsons, T. (1995). Tectonic implications of post-30 Ma Pacific and North American relative plate motions. *GSA Bulletin*, 107(8), 937–959. [https://doi.org/10.1130/0016-7606\(1995\)107<937:TIOPMP>2.3.CO;2](https://doi.org/10.1130/0016-7606(1995)107<937:TIOPMP>2.3.CO;2)
- Bostock, M. G., Royer, A. A., Hearn, E. H., & Peacock, S. M. (2012). Low frequency earthquakes below southern Vancouver Island. *Geochemistry, Geophysics, Geosystems*, 13(11). <https://doi.org/10.1029/2012gc004391>
- Brudzinski, M. R., & Allen, R. M. (2007). Segmentation in episodic tremor and slip all along Cascadia. *Geology*, 35(10), 907–910. <https://doi.org/10.1130/G23740A.1>
- Castillo, D. A., & Ellsworth, W. L. (1993). Seismotectonics of the San Andreas Fault system between Point Arena and Cape Mendocino in northern California: Implications for the development and evolution of a young transform. *Journal of Geophysical Research*, 98(B4), 6543–6560. <https://doi.org/10.1029/92JB02866>
- Chamberlain, C. J., Shelly, D. R., Townend, J., & Stern, T. A. (2014). Low-frequency earthquakes reveal punctuated slow slip on the deep extent of the Alpine Fault, New Zealand. *Geochemistry, Geophysics, Geosystems*, 15(7), 2984–2999. <https://doi.org/10.1002/2014GC005436>
- Dickinson, W. R., & Snyder, W. S. (1979). Geometry of subducted slabs related to San Andreas transform. *The Journal of Geology*, 87(6), 609–627. <https://doi.org/10.1086/628456>
- Dragert, H., Wang, K., & James, T. S. (2001). A silent slip event on the deeper Cascadia subduction interface. *Science*, 292(5521), 1525–1528. <https://doi.org/10.1126/science.1060152>
- Frank, W. B. (2016). Slow slip hidden in the noise: The intermittence of tectonic release. *Geophysical Research Letters*, 43(19), 10125–10133. <https://doi.org/10.1002/2016GL069537>
- Furlong, K. P., & Govers, R. (1999). Ephemeral crustal thickening at a triple junction: The Mendocino crustal conveyor. *Geology*, 27(2), 127–130. [https://doi.org/10.1130/0091-7613\(1999\)027<0127:ECTAAT>2.3.CO;2](https://doi.org/10.1130/0091-7613(1999)027<0127:ECTAAT>2.3.CO;2)

- Furlong, K. P., Lock, J., Guzofski, C., Whitlock, J., & Benz, H. (2003). The Mendocino crustal conveyor: Making and breaking the California crust. *International Geology Review*, 45(9), 767–779. <https://doi.org/10.2747/0020-6814.45.9.767>
- Furlong, K. P., Villaseñor, A., Benz, H. M., & McKenzie, K. A. (2024). Formation and evolution of the Pacific-North American (San Andreas) plate boundary: Constraints from the crustal architecture of Northern California. *U.S. Geological Survey Data Release*, 43(6), e2023TC007963. <https://doi.org/10.5066/P14QGYIY>
- Ghosh, A., Vidale, J. E., Sweet, J. R., Creager, K. C., Wech, A. G., Houston, H., & Brodsky, E. E. (2010). Rapid, continuous streaking of tremor in Cascadia. *Geochemistry, Geophysics, Geosystems*, 11(12), Q12010. <https://doi.org/10.1029/2010GC003305>
- Gibbons, S. J., & Ringdal, F. (2006). The detection of low magnitude seismic events using array-based waveform correlation. *Geophysical Journal International*, 165(1), 149–166. <https://doi.org/10.1111/j.1365-246X.2006.02865.x>
- Guo, H., Atterholt, J. W., McGuire, J. J., & Thurber, C. (2024). Evidence for low effective stress within the crust of the subducted Gorda plate from the 2022 December Mw 6.4 Ferndale earthquake sequence. *Seismological Research Letters*, 96(3), 1504–1520. <https://doi.org/10.1785/0220240078>
- Hayes, G. P., Moore, G. L., Portner, D. E., Hearne, M., Flamme, H., Furtney, M., & Smoczyk, G. M. (2018). Slab2, a comprehensive subduction zone geometry model. *Science*, 362(6410), 58–61. <https://doi.org/10.1126/science.aat4723>
- Hole, J. A., Beaudoin, B. C., & Henstock, T. J. (1998). Wide-angle seismic constraints on the evolution of the deep San Andreas plate boundary by Mendocino triple junction migration. *Tectonics*, 17(5), 802–818. <https://doi.org/10.1029/98TC02261>
- Ide, S. (2016). Characteristics of slow earthquakes in the very low frequency band: Application to the Cascadia subduction zone. *Journal of Geophysical Research: Solid Earth*, 121(8), 5942–5952. <https://doi.org/10.1002/2016JB013085>
- Ide, S., & Yabe, S. (2014). Universality of slow earthquakes in the very low frequency band. *Geophysical Research Letters*, 41(8), 2786–2793. <https://doi.org/10.1002/2014GL059712>
- Ide, S., Shelly, D. R., & Beroza, G. C. (2007). Mechanism of deep low frequency earthquakes: Further evidence that deep non-volcanic tremor is generated by shear slip on the plate interface. *Geophysical Research Letters*, 34(3), L03308. <https://doi.org/10.1029/2006GL028890>
- Ide, S., Yabe, S., Tai, H.-J., & Chen, K. H. (2015). Thrust-type focal mechanisms of tectonic tremors in Taiwan: Evidence of subduction. *Geophysical Research Letters*, 42(9), 3248–3256. <https://doi.org/10.1002/2015GL063794>
- Jachens, R. C., & Griscom, A. (1983). Three-dimensional geometry of the Gorda plate beneath northern California. *Journal of Geophysical Research*, 88(B11), 9375–9392. <https://doi.org/10.1029/JB088iB11p09375>
- McCrory, P. A., Blair, J. L., Oppenheimer, D. H., & Walter, S. R. (2006). Depth to the Juan De Fuca slab beneath the Cascadia subduction margin—A 3-D model for sorting earthquakes. *U.S. Geol. Surv. Data Ser.*, 91. Retrieved from <http://pubs.usgs.gov/ds/91/>
- McCrory, P. A., Blair, J. L., Waldhauser, F., & Oppenheimer, D. H. (2012). Juan de Fuca slab geometry and its relation to Wadati-Benioff zone seismicity. *Journal of Geophysical Research*, 117(B9), B09306. <https://doi.org/10.1029/2012JB009407>
- McCrory, P. A., Wilson, D. S., & Stanley, R. G. (2009). Continuing evolution of the Pacific–Juan de Fuca–North America slab window system—A trench–ridge–transform example from the Pacific Rim. *Tectonophysics*, 464(1), 30–42. <https://doi.org/10.1016/j.tecto.2008.01.018>
- McKenzie, K. A., Furlong, K. P., & Kirby, E. (2022). Mid-miocene to present upper-plate deformation of the southern Cascadia forearc: Effects of the superposition of subduction and transform tectonics. *Frontiers in Earth Science*, 10, 832515. <https://doi.org/10.3389/feart.2022.832515>
- Miller, M. M., Melbourne, T., Johnson, D. J., & Sumner, W. Q. (2002). Periodic slow earthquakes from the Cascadia subduction zone. *Science*, 295(5564), 2423. <https://doi.org/10.1126/science.1071193>
- Nuyen, C., & Schmidt, D. (2024). Along-strike changes in ETS behavior near the slab edge of Southern Cascadia. *Seismica*, 2(4). <https://doi.org/10.26443/seismica.v2i4.1097>
- Plourde, A. P., Bostock, M. G., Audet, P., & Thomas, A. M. (2015). Low-frequency earthquakes at the southern Cascadia margin. *Geophysical Research Letters*, 42(12), 4849–4855. <https://doi.org/10.1002/2015GL064363>
- Rogers, G., & Dragert, H. (2003). Episodic tremor and slip on the Cascadia subduction zone: The chatter of silent slip. *Science*, 300(5627), 1942–1943. <https://doi.org/10.1126/science.1084783>
- Roussel, B., Bürgmann, R., & Campillo, M. (2019). Slow slip events in the roots of the San Andreas fault. *Science Advances*, 5(2), eaav3274. <https://doi.org/10.1126/sciadv.aav3274>
- Royer, A. A., & Bostock, M. G. (2014). A comparative study of low frequency earthquake templates in northern Cascadia. *Earth and Planetary Science Letters*, 402, 247–256. <https://doi.org/10.1016/j.epsl.2013.08.040>
- Shelly, D. R. (2010). Migrating tremors illuminate complex deformation beneath the seismogenic San Andreas fault. *Nature*, 463(7281), 648–652. <https://doi.org/10.1038/nature08755>
- Shelly, D. R. (2025). A catalog of low-frequency earthquakes at the southern edge of Cascadia subduction [Dataset]. *U.S. Geological Survey Data Release*. <https://doi.org/10.5066/P1TCKK7G>
- Shelly, D. R., & Hardebeck, J. L. (2010). Precise tremor source locations and amplitude variations along the lower-crustal central San Andreas Fault. *Geophysical Research Letters*, 37(14), L14301. <https://doi.org/10.1029/2010GL043672>
- Shelly, D. R., & Johnson, K. M. (2011). Tremor reveals stress shadowing, deep postseismic creep, and depth-dependent slip recurrence on the lower-crustal San Andreas Fault near Parkfield. *Geophysical Research Letters*, 38(13), L13312. <https://doi.org/10.1029/2011GL047863>
- Shelly, D. R., Beroza, G. C., & Ide, S. (2007). Non-volcanic tremor and low-frequency earthquake swarms. *Nature*, 446(7133), 305–307. <https://doi.org/10.1038/nature05666>
- Shelly, D. R., Beroza, G. C., Ide, S., & Nakamura, S. (2006). Low-frequency earthquakes in Shikoku, Japan, and their relationship to episodic tremor and slip. *Nature*, 442(7099), 188–191. <https://doi.org/10.1038/nature04931>
- Smith, S. W., Knapp, J. S., & McPherson, R. C. (1993). Seismicity of the Gorda plate, structure of the continental margin, and an eastward jump of the Mendocino triple junction. *Journal of Geophysical Research*, 98(B5), 8153–8171. <https://doi.org/10.1029/93JB00026>
- Sweet, J. R., Creager, K. C., & Houston, H. (2014). A family of repeating low-frequency earthquakes at the downdip edge of tremor and slip. *Geochemistry, Geophysics, Geosystems*, 15(9), 3713–3721. <https://doi.org/10.1002/2014GC005449>
- Szeliga, W., Melbourne, T. I., Miller, M. M., & Santillan, V. M. (2004). Southern Cascadia episodic slow earthquakes. *Geophysical Research Letters*, 31(16), L16602. <https://doi.org/10.1029/2004GL020824>
- Thomas, A. M., & Bostock, M. G. (2015). Identifying low-frequency earthquakes in central Cascadia using cross-station correlation. *Tectonophysics*, 658, 111–116. <https://doi.org/10.1016/j.tecto.2015.07.013>
- Thomas, A. M., Bürgmann, R., Shelly, D. R., Beeler, N. M., & Rudolph, M. L. (2012). Tidal triggering of low frequency earthquakes near Parkfield, California: Implications for fault mechanics within the brittle-ductile transition. *Journal of Geophysical Research*, 117(B5), B05301. <https://doi.org/10.1029/2011JB009036>
- Thurber, C., Zhang, H., Waldhauser, F., Hardebeck, J., Michael, A., & Eberhart-Phillips, D. (2006). Three-dimensional compressional wavespeed model, earthquake relocations, and focal mechanisms for the Parkfield, California, region. *Bulletin of the Seismological Society of America*, 96(4B), S38–S49. <https://doi.org/10.1785/012005050825>

- Verdonck, D., & Zandt, G. (1994). Three-dimensional crustal structure of the Mendocino triple Junction region from local earthquake travel times. *Journal of Geophysical Research*, 99(B12), 23843–23858. <https://doi.org/10.1029/94JB01238>
- Waldhauser, F., & Ellsworth, W. L. (2000). A double-difference earthquake location algorithm: Method and application to the northern Hayward fault, California. *Bulletin of the Seismological Society of America*, 90(6), 1353–1368. <https://doi.org/10.1785/0120000006>
- Wech, A. G. (2021). Cataloging tectonic tremor energy radiation in the Cascadia subduction zone. *Journal of Geophysical Research: Solid Earth*, 126(10), e2021JB022523. <https://doi.org/10.1029/2021JB022523>
- Wech, A. G., & Creager, K. C. (2007). Cascadia tremor polarization evidence for plate interface slip. *Geophysical Research Letters*, 34(22), L22306. <https://doi.org/10.1029/2007GL031167>
- Wech, A. G., & Creager, K. C. (2008). Automated detection and location of Cascadia tremor. *Geophysical Research Letters*, 35(20), L20302. <https://doi.org/10.1029/2008GL035458>
- Wech, A. G., & Creager, K. C. (2011). A continuum of stress, strength and slip in the Cascadia subduction zone. *Nature Geoscience*, 4(9), 624–628. <https://doi.org/10.1038/ngeo1215>
- Wech, A. G., Boese, C. M., Stern, T. A., & Townend, J. (2012). Tectonic tremor and deep slow slip on the Alpine Fault. *Geophysical Research Letters*, 39(10), L10303. <https://doi.org/10.1029/2012GL051751>
- Wessel, P., Luis, J. F., Uieda, L., Scharroo, R., Wobbe, F., Smith, W. H. F., & Tian, D. (2019). The generic mapping tools version 6. *Geochemistry, Geophysics, Geosystems*, 20(11), 5556–5564. <https://doi.org/10.1029/2019GC008515>
- Wilson, D. S. (1989). Deformation of the so-called Gorda plate. *Journal of Geophysical Research*, 94(B3), 3065–3075. <https://doi.org/10.1029/JB094iB03p03065>
- Yoon, C. E., & Shelly, D. R. (2024). Distinct yet adjacent earthquake sequences near the Mendocino triple junction: 20 December 2021 Mw 6.1 and 6.0 Petrolia, and 20 December 2022 Mw 6.4 Ferndale. *The Seismic Record*, 4(1), 81–92. <https://doi.org/10.1785/0320230053>

## References From the Supporting Information

- Beaucé, E., Frank, W. B., & Romanenko, A. (2017). Fast matched filter (FMF): An efficient seismic matched-filter search for both CPU and GPU architectures. *Seismological Research Letters*, 89(1), 165–172. <https://doi.org/10.1785/0220170181>
- Shelly, D. R., Ellsworth, W. L., & Hill, D. P. (2016). Fluid-faulting evolution in high definition: Connecting fault structure and frequency-magnitude variations during the 2014 Long Valley Caldera, California, earthquake swarm. *Journal of Geophysical Research: Solid Earth*, 121(3), 1776–1795. <https://doi.org/10.1002/2015JB012719>